CHEMISTRY OF MATERIALS

ARTICLE

pubs.acs.org/cm

Unexpected Mechanism of Zn^{2+} Insertion in Calcium Phosphate Bioceramics

Sandrine Gomes,[†,‡] Jean-Marie Nedelec,[†,‡] Edouard Jallot,[§] Denis Sheptyakov,[⊥] and Guillaume Renaudin*[,†,‡]

[†]Clermont Université, ENSCCF, Laboratoire des Matériaux Inorganiques, BP 10448, 63000 Clermont-Ferrand, France

[‡]CNRS, UMR 6002, LMI, 63177 Aubière, France

[§]Clermont Université, Université Blaise Pascal, CNRS/IN2P3, Laboratoire de Physique Corpusculaire, BP 10448, 63000 Clermont-Ferrand, France

[⊥]Laboratory for Neutron Scattering, Paul Scherrer Institut, 5235 Villigen PSI, Switzerland

ABSTRACT: Rietveld analysis on X-ray powder diffraction patterns recorded from Zn-doped, Zn/Sr, and Zn/Mg codoped biphasic calcium phosphate (BCP) samples has been used to locate Zn^{2+} cations in both hydroxyapatite (HAp) and β-tricalcium phosphate (β-TCP) phases heat-treated at 1100 °C. Zn atoms occupy interstitial sites in HAp (Wyckoff site 2*b*), leading to an insertion solid solution of general composition $Ca_{10}Zn_x(PO_4)_6O_{2x}(OH)_{2-2x}$. Replacement of hydroxyl by O^{2-} anions with formation of linear O−Zn−O entities should be considered to preserve the electroneutrality of the material. Contrary to HAp case, Zn atoms substitute calcium atoms in β-TCP leading to a substitution solid solution of general composition $Ca_{3-x}Zn_x(PO_4)_2$. Micro-Raman spectroscopy and neutron diffraction have confirmed these insertion/substitution mechanisms. The different mechanisms of zinc incorporation should be considered to stabilize the desired calcium phosphate phase which are managed by the Ca/P and (Ca+Zn)/P ratios. Furthermore, discussion of biological properties of Zn-doped calcium phosphate ceramics should take into account the true insertion mechanism as critically discussed here.

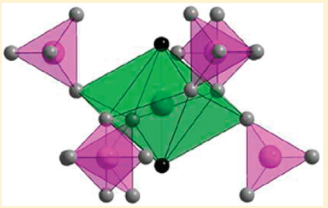

KEYWORDS: biomaterials, zinc doping, calcium phosphates, Rietveld refinement, Raman

1-. INTRODUCTION

It is well-known that bone mineral mass is dominated by nanocrystalline nonstoichiometric hydroxyapatite (HAp, $Ca_{10}(PO_4)_6(OH)_2$), and whitlockite—the Mg-incorporated β-tricalcium phosphate (β-TCP, β-$Ca_3(PO_4)_2$)—can be found at many different sites in the human body.[1−3] For these reasons and because of the difference in the solubility of the two calcium phosphate phases, biphasic calcium phosphates (BCP), composed of a mixture of hydroxyapatite and β-tricalcium phosphate, are interesting biocompatible materials for reconstructive surgery and for bone prosthesis coatings.[4] Another interesting possibility is to perform ionic substitution in calcium phosphates to prepare materials with specific properties, such as anti-inflammatory, anti-osteroporotic, or antibacterial. The incorporation of specific doping elements can then be used to tune the biological properties of BCP. More recently, the possibility to realize codoping with at least two distinct elements has been put forward.[5,6]

Various ionic species can be included in bone apatite and the level of ionic substitution varies from the weight percent level for carbonate substitution[7] to the parts per million level for strontium or barium.[8] The role of many of these ionic species in hard tissues is not fully understood because of the difficulties encountered in monitoring and quantifying their proportions, which vary according to dietary alteration, and to physiological and pathological causes.[9] However, it is commonly accepted that these different ions play a major role in the biochemistry of bones, enamel and dentin[8] by a substitution process (and not a catalytic one[10]). Zinc substitution in HAp has been the focus of particular interest because of its presence in all biological tissues and its diverse roles in biological functions, such as enzyme activity, nucleic acid metabolism, maintenance of membrane structure and function, hormonal activity, as well as biomineralization[11] and potentially pathological calcifications (either concretion or ectopic calcification) often associated with tissue alteration.[10,12] The uptake and release of Zn in the body are strongly mediated by the bone reservoir, where the Zn content ranges from 125 to 250 ppm (against 28−33 ppm for whole body).[13] It has been demonstrated that zinc has a stimulatory effect on bone formation and mineralization in vivo and in vitro,[14,15] and that Zn incorporation into implants promotes bone formation around the material,[16−19] improves biological properties,[16,20] decreases the inflammatory response,[21,22] and has an antibacterial effect.[23]

To understand the mechanisms of incorporation of doping elements in HAp, and to correctly characterize natural and/or pathological nanocrystalline multisubstituted apatite materials, it is of great importance to perform detailed structural characterizations of substituted synthetic HAp, as well as BCP. Our previous studies on strontium, magnesium and silicon incorporation into BCP samples have highlighted their microstructural effects and their preferential crystallographic sites.[24−27] In

Received: February 21, 2011
Revised: May 13, 2011
Published: May 31, 2011

Table 1. Comparison of Bivalent Cation's Ionic Radii, Ca^{2+}, Mg^{2+}, Sr^{2+}, and Zn^{2+}, for Different Common Coordination Numbers According to Shannon[28]

	ionic radius (Å)			
coordination no.	Ca^{2+}	Mg^{2+}	Sr^{2+}	Zn^{2+}
4		0.57		0.60
6	1.00	0.72	1.18	0.74
7	1.06		1.21	
8	1.12	0.89	1.26	0.90
9	1.18		1.31	

comparison to Ca^{2+}, Mg^{2+} and Sr^{2+}, which are small and large cations, respectively, present different mechanisms of incorporation in BCP samples.[24−26] Considering only the ionic radii,[28] Zn^{2+} should behave similarly to Mg^{2+} (see Table 1). Contrary to the behavior of the strontium cation, which displays a total solid solution $Ca_{10-x}Sr_x(PO_4)_6OH_2$ with $0 \le x \le 10$, the magnesium cation is barely incorporated in the HAp structure and stabilizes the β-TCP phase at the expense of HAp.[24−26]

Incorporation of Zn into the HAp structure, as well as other metallic elements such as Pb, Cd, Mn, Ag, Co, Ni, or Cu has been mentioned in numerous studies.[13,19,29−39] There has been a number of contradictory reports on Zn^{2+} incorporation in HAp; namely about its solubility, ranging from a few mole percent to 15 mol %,[40−42] about the Zn atoms location, sorbed on the HAp surface (either 6-fold or 4-fold coordinated), or incorporated in one of the two crystallographic Ca sites (the 9-fold coordinated Ca1 and the 7-fold coordinated Ca2 sites) of HAp structure.[30,33,34,38,40] Few X-ray diffraction analyses have been performed on Zn-substituted calcium phosphate samples with complete Rietveld analysis (i.e., with detailed structure information).[29,40,43,44] Recent literature is mainly focused on theoretical modeling (Density Functional Theory calculation, first principles total energy calculation) and X-ray absorption spectroscopy (EXAFS and XANES) to characterize the local environment of Zn incorporated in HAp.[33,45−49] Tang et al.[33] indicate that Zn substitutes preferentially in the Ca2 site, rather than in the Ca1 site, and prefers tetrahedral coordination (which suggests an enormous distortion of the neighboring HAp structure where the Ca2 site is normally 7-fold coordinated). Although, the tetrahedral coordination is also supported by the work of Bazin et al. on pathological apatite,[46] it is nevertheless concluded that Zn is localized at the surface and not into the structure of apatite. The preference for Zn substitution into the Ca2 site is also supported by results presented by Matsunaga et al.[45] with a highlighted role played by Ca^{2+} vacancies. The recent literature shows the importance of the knowledge of the trace elements location, especially oligo-elements, in calcium phosphates to understand mechanisms of incorporation and/or release and the associated pathologies or biological role. The present study aims to investigate directly the crystallographic structure of Zn-doped BCP samples by using Rietveld analyses performed on X-ray powder diffraction patterns (the electronic contrast between Zn^{2+} and Ca^{2+}, with a ratio of 1.5 in X-ray scattering factors, is adapted to localize Zn atoms in calcium phosphates). Neutron powder diffraction and micro-Raman spectroscopy were used to strenghen results.

Study of Zn−Mg and Zn−Sr cosubstituted BCP samples will also allow determining if knowledge of mechanism of incorporation of single element (Mg, Sr, Zn) in BCP can be used to predict the behavior in multisubstituted BCP and thus allow a more rational design of multifunctional Bioceramics.

2-. MATERIALS AND METHODS

2.1. Sol−Gel Elaboration of Zn-Substituted BCP Samples. The sol−gel route was used to synthesize Zn-doped BCP samples.[20,22] Briefly, to produce 2 g of pure HAp powder, 4.7 g of $Ca(NO_3)_2.4H_2O$ (Aldrich) and 0.84 g of P_2O_5 (Avocado Research chemicals) were dissolved in anhydrous ethanol under stirring and refluxed at 85 °C for 24 h. Then, this solution was kept at 55 °C for 24 h, to obtain a white consistent gel and further heated at 80 °C for 10 h to obtain a white powder. Finally, this powder was heated at 1100 °C during 15 h. To prepare Zn-substituted samples, the required amounts of $Zn(NO_3)_2.6H_2O$ (Acros Organics) was added to the solution, simultaneously with $Ca(NO_3)_2.4H_2O$. Nominal compositions have been calculated assuming substituted stoichiometric hydroxyapatite; i.e. (Ca+Zn)/P = 1.67. In the following, samples are labeled "BCP" instead of "HAp", due to the β-TCP-stabilizing effect of Zn (as already mentioned in the literature[13,19,40,44]) leading to a mixture of HAp and β-TCP phases when introducing Zn.

Eight samples have been prepared: 1/an undoped biphasic calcium phosphate sample (named $Zn_{0.00}$-BCP in the following) of nominal composition $Ca_{10}(PO_4)_6(OH)_2$; 2/five Zn-substituted BCP samples, $Zn_{0.25}$-BCP, $Zn_{0.50}$-BCP, $Zn_{1.00}$-BCP, $Zn_{1.50}$-BCP, $Zn_{2.00}$-BCP of nominal composition $Ca_{10-x}Zn_x(PO_4)_6(OH)_2$ (with x = 0.25, 0.5, 1.0, 1.5, and 2.0 respectively); 3/one Zn and Mg cosubstituted BCP sample (named $Zn_{0.25}Mg_{0.25}$-BCP) of nominal composition $Ca_{9.5}Zn_{0.25}Mg_{0.25}(PO_4)_6(OH)_2$; 4/and one Zn and Sr cosubstituted BCP sample (named $Zn_{0.25}Sr_{0.25}$-BCP) of nominal composition $Ca_{9.5}Zn_{0.25}Sr_{0.25}(PO_4)_6(OH)_2$. The Zn-substitution levels correspond to 2.5 (x = 0.25), 5.0 (x = 0.5), 10.0 (x = 1.0), 15 (x = 1.5) and 20 (x = 2.0) atomic percents (at %) of calcium by using a nominal (Ca+Zn)/P ratio of 1.67. The cosubstituted samples correspond to the incorporation of 2.5 at. % of zinc with 2.5 at. % of either magnesium or strontium; corresponding to the nominal (Ca+Zn+A)/P ratio of 1.67 (with A = Mg or Sr).

2.2. X-ray Powder Diffraction (XRPD). XRPD patterns were recorded on an X'Pert Pro PANalytical (Almelo, Netherlands) diffractometer, with $\theta-\theta$ geometry, equipped with a solid detector X-Celerator and using Cu Kα radiation (λ = 1.54184 Å). XRPD patterns were recorded at room temperature in the interval $3° < 2\theta < 120°$, with a step size of $\Delta 2\theta = 0.0167°$ and a counting time of 200 s for each data value. A total counting time of about 200 min was used for each sample. An XRPD pattern was collected from a pure LaB_6 NIST standard (SRM 660b) by using the same experimental conditions in order to extract the instrumental resolution function to improve the peak profile fitting and to extract intrinsic microstructural parameters of both HAp and β-TCP phases.

2.3. Neutron Powder Diffraction (NPD). NPD experiment was performed with the high resolution − high intensity HRPT diffractometer[50] at SINQ/PSI (Villigen, Switzerland) at room temperature. The sample $Zn_{0.50}$-BCP (~1 g mass) was enclosed in cylindrical vanadium containers of ~6 mm diameter and measured at two different wavelengths (λ = 1.494 Å and 1.886 Å) in the 2θ range 4−165° with a step size of $2\theta = 0.05°$. Transmission factor was calculated ($\mu R = 0.15$) and data corrected accordingly. The low amount of hydrogen atoms in the samples allows recording NPD patterns with acceptable background without preparing deuterated sample.

2.4. Rietveld Analyses. Rietveld refinements of X-ray powder patterns were performed for each sample with the program FullProf.2k.[51] The large X-ray scattering factor of zinc, compared to others Ca, P, O and H atoms, was advantageously use to locate Zn

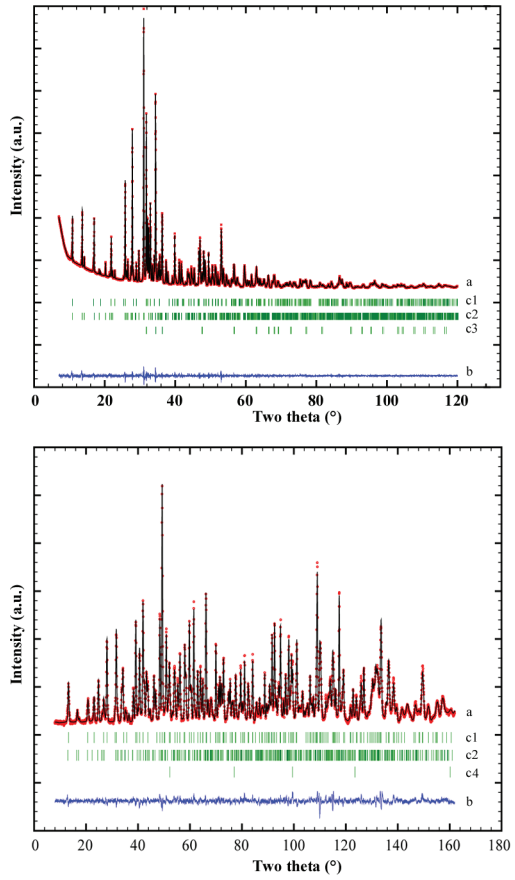

Figure 1. Rietveld plots for XRPD from $Zn_{1.00}$-BCP (top; λ = 1.54184 Å) and NPD from $Zn_{0.50}$-BCP (bottom; λ = 1.494 Å) samples: (a) experimental (red dots) and calculated (black lines), (b) difference curves, and Bragg peak positions for HAp (c1), β-TCP (c2), ZnO (c3), and vanadium (c4).

crystallographic sites. The procedure used (both data-collection and refinement strategy) corresponds to the general guidelines for structure refinement using the Rietveld (whole-profile) method formulated by the International Union of Crystallography Commission on Powder Diffraction.[52−54] The initial structural parameters of hydroxyapatite, $Ca_{10}(PO_4)_6(OH)_2$, were taken from:[55] space group $P6_3/m$, Z = 1, a = 9.4218 Å, and c = 6.8813 Å, 7 independent atomic positions: two Ca positions in sites 4*f* (z = 0.0007) and 6*h* (x = 0.2465, y = 0.9933), one P position in site 6*h* (x = 0.3968, y = 0.3693), and four O positions in sites 6*h* (x = 0.331, y = 0.480 and x = 0.579, y = 0.455), 12*i* (x = 0.3394, y = 0.2569, z = 0.0694) and 4*e* (z = 0.192 with a half occupancy). The initial structural parameters of β-TCP, $Ca_3(PO_4)_2$, were taken from:[56] space group *R*3*c*, Z = 21, a = 10.4352 Å and c = 37.4029 Å, 18 independent atomic positions: five Ca positions (three in site 18*b* and two in site 6*a* at one-half occupancy), three P positions (two in site 18*b* and one in site 6*a*), and ten O positions (nine in site 18*b* and one in site 6*a*). Zincite, ZnO, was the third phase taken into account during Rietveld analyses for samples $Zn_{1.00}$-BCP, $Zn_{1.50}$-BCP and $Zn_{2.00}$-BCP. Initial structural parameters of zincite were taken from.[57]

The following parameters were first refined: scale factors, zero shift, line profile parameters, lattice parameters, preferential orientations and asymmetry parameters. In a second step, atomic displacement factors were refined (only three thermal displacement values were considered, one for divalent cations, one for P, and one for O, in order to avoid strong correlation between site occupancies and atomic displacement factors[52−54]), as well as atomic coordinates when the proportion of the phase was considered to be significant. Site occupancies of cations, phosphate, and hydroxyl anions were systematically checked in the last runs. Figure 1 top shows, as an example, the Rietveld plot obtained for $Zn_{1.00}$-BCP sample containing the three HAp, β-TCP, and ZnO phases.

Joint Rietveld refinement on the two NPD patterns (λ = 1.494 and 1.886 Å) recorded for $Zn_{0.50}$-BCP was performed in order to strengthen the location of Zn atoms (previously extracted from XRPD Rietveld analyses) by confronting atomic occupancy parameters based on electronic density (XRPD) and on nucleus (NPD) population. Figure 1 bottom shows the Rietveld plot obtained for $Zn_{0.50}$-BCP with λ = 1.494 Å. The neutron patterns showed the same phases as those observed by X-ray diffraction. There is no justification, here, to perfom joint Rietveld refinement on XRPD and NPD simultaneously (NPD was used to strengthen results from XRPD).

2.5. Micro-Raman Spectroscopy. Micro-Raman spectra were recorded at room temperature using a Jobin-Yvon T64000 device. The spectral resolution obtained with an excitation source at 514.5 nm (argon ion laser line, Spectra Physics 2017) is about 1 cm^{-1}. The Raman detector was a charge coupled device (CCD) multichannel detector cooled by liquid nitrogen to 140 K. The laser beam was focused onto the sample through an Olympus confocal microscope with 10× (corresponding to the whole sample) and x100 (selected area corresponding to single phase enriched region) magnifications. Measured power at the sample level was kept low (less than 10 mW) in order to avoid any damage of the material. The Raman scattered light was collected with the microscope objective at 180° from the excitation and filtered with an holographic Notch filter before being dispersed by a single grating (1800 grooves per mm). Spectra were recorded in the frequencies ranges 100−1500 cm^{-1} and 3000−3800 cm^{-1} in order to investigate respectively the vibration modes of phosphate and hydroxyl stretching. Spectra were analyzed by a profile fitting procedure using a Lorentzian function.

3-. RESULTS

Elemental analysis of the samples by ICP-AES confirms the global nominal compositions as usually observed when using sol−gel route. The refined chemical compositions of the synthesized powders were extracted from the Rietveld refinement results by taking into account the quantitative phase analysis and the refined composition for each phase to calculate a refined bulk composition. Nominal and refined compositions are in fairly good agreement as indicated in Table 2. The similarities between nominal and refined bulk ratios; Ca/P, (Ca+Zn)/P and (Ca+Zn+*A*)/P in Table 2, testify not only the success of the synthesis process but also to the accuracy of the Rietveld refinement procedure. Energy-dispersive spectrometer (EDS) coupled on a scanning electronic microscope (SEM) has shown that Ca, P, and Zn were the only present elements (without considering oxygen).

3.1. Quantitative Phase Analysis. Results from the quantitative analysis extracted from Rietveld refinements from XRPD patterns are presented in Figure 2, and weight percent (wt %) values are gathered in Table 3. Adequate use of a whole-pattern refinement procedure led to accurate quantitative phase determination, namely in the case of our samples with absence of absorption contrast between phases.[58,59] Standard deviations, corresponding to σ values given by the FullProf output files,[51] are indicated in parentheses in the Tables 3−5, and accuracy can be estimated as being 3σ althought it is not the 'true' error in the analyses.[52] Then an estimated error of 1 wt % can be considered here for each phase proportion. The already described Zn-stabilizing feature for β-TCP,[19,39,43,60] at the expense of HAp,

Table 2. Nominal and Refined Compositions (Ca, P, Zn, Mg, Sr) for the Eight Samples of Nominal General Formula $Ca_{10-x-y}Zn_xA_y(PO_4)_6(OH)_2$ (with A = Mg, Sr)[a]

	$Zn_{0.00}$-BCP	$Zn_{0.25}$-BCP	$Zn_{0.50}$-BCP	$Zn_{1.00}$-BCP	$Zn_{1.50}$-BCP	$Zn_{2.00}$-BCP	$Zn_{0.25}Mg_{0.25}$-BCP	$Zn_{0.25}Sr_{0.25}$-BCP
Ca nominal (wt %)	39.9	38.7	37.5	35.0	32.5	30.4	37.8	37.2
Ca refined (wt %)	39.8 (2)	38.6 (2)	38.1 (2)	35.4 (2)	32.5 (2)	30.6 (2)	38.2 (2)	37.9 (2)
P nominal (wt %)	18.5	18.4	18.3	18.0	17.7	17.6	18.5	18.2
P refined (wt %)	18.6 (1)	18.8 (1)	18.7 (1)	18.3 (1)	18.0 (1)	17.7 (1)	18.8 (1)	18.2 (1)
Zn nominal (wt %)		1.6	3.2	6.3	9.4	12.4	1.6	1.6
Zn refined (wt %)		1.8 (2)	2.6 (3)	6.6 (6)	10.6 (9)	13 (1)	1.6 (2)	1.3 (2)
Mg nominal (wt %)							0.6	
Mg refined (wt %)							0.30 (5)	
Sr nominal (wt %)								2.1
Sr refined (wt %)								2.0 (2)
Ca/P nominal	1.67	1.63	1.58	1.50	1.42	1.33	1.58	1.58
Ca/P refined	1.65 (2)	1.59 (2)	1.57 (2)	1.49 (2)	1.40 (2)	1.34 (2)	1.57 (2)	1.61 (2)
(Ca+Zn)/P nominal	1.67	1.67	1.67	1.67	1.67	1.67	1.62	1.62
(Ca+Zn)/P refined	1.65 (2)	1.63 (2)	1.64 (2)	1.66 (3)	1.67 (4)	1.68 (4)	1.61 (4)	1.64 (4)
(Ca+A)/P nominal	1.67	1.62	1.58	1.50	1.42	1.33	1.62	1.62
(Ca+A)/P refined	1.65 (2)	1.59 (2)	1.57 (2)	1.49 (2)	1.40 (2)	1.34 (2)	1.59 (5)	1.65 (4)
(Ca+Zn+A)/P nominal	1.67	1.67	1.67	1.67	1.67	1.67	1.67	1.67
(Ca+Zn+A)/P refined	1.65 (2)	1.63 (2)	1.64 (2)	1.66 (3)	1.67 (4)	1.68 (4)	1.63 (7)	1.68 (6)
x nominal		0.25	0.50	1.00	1.50	2.00	0.25	0.25
x refined		0.28 (3)	0.40 (5)	1.02 (9)	1.6 (1)	2.1 (2)	0.25 (3)	0.20 (3)
y nominal							0.25	0.25
y refined							0.13 (4)	0.23 (3)

[a] Errors on the last digit indicated in parentheses are calculated considering standard deviations from Rietveld analyses.

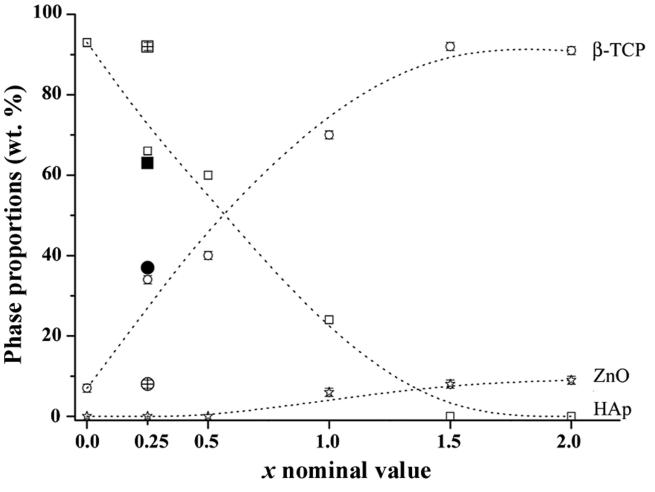

Figure 2. Quantitative Rietveld analysis extracted from XRPD patterns: squares, circles and stars correspond to HAp, β-TCP, and ZnO, respectively. Zn-doped BCP samples are represented by open symbols and cosubstituted samples, Zn−Mg and Zn−Sr are represented by solid and crossed symbols, respectively. Dotted lines are drawn only as guides for the eyes and correspond to the single Zn-BCP series (without taking into account cosubstituted samples). Error bars are represented, but are within symbols.

is clearly demonstrated by the series of the single Zn-substituted samples (Zn_x-BCP samples with x = 0.00, 0.25, 0.50, 1.00, 1.50 and 2.00), as illustrated by dotted lines in Figure 2. The undoped BCP sample is mainly composed of HAp (93 wt % HAp, and 7 wt % β-TCP). This situation is quickly reversed: $Zn_{1.00}$-BCP contains

Table 3. Results of the Quantitative Analyses (wt %) Extracted from Rietveld Refinements; Standard Deviations, Corresponding to σ Values Given by FullProf Output Files Are Indicated in Parentheses (accuracy can be estimated as being 3σ)[a]

sample	HAp (wt %)	β-TCP (wt %)	ZnO (wt %)
$Zn_{0.00}$-BCP	93.0 (2)	7.0 (2)	
$Zn_{0.25}$-BCP	66.1 (3)	33.9 (3)	
$Zn_{0.50}$-BCP	59.8 (3)	40.2 (3)	
$Zn_{0.50}$-BCP	*60 (1)*	*40 (1)*	
$Zn_{1.00}$-BCP	23.7 (3)	69.9 (3)	6.4 (3)
$Zn_{1.50}$-BCP		92.0 (3)	8.0 (3)
$Zn_{2.00}$-BCP		90.9 (3)	9.1 (3)
$Zn_{0.25}Mg_{0.25}$-BCP	62.7 (3)	37.3 (3)	
$Zn_{0.25}Sr_{0.25}$-BCP	92.0 (3)	8.0 (3)	

[a] Italic characters correspond to values extracted from Rietveld refinement on neutron patterns for $Zn_{0.50}$-BCP.

only 24 wt % of HAp, whereas $Zn_{1.50}$-BCP and $Zn_{2.00}$-BCP sample contain no HAp at all. These last two samples are only composed of the β-tricalcium phosphate phase and zincite, indicating that β-TCP is apparently not allowed to incorporate the entire nominal Zn proportion. In fact, the complete disappearance of the HAp phase, replaced by a large proportion of ZnO, seems to indicate that the ratio (Ca+Zn)/P, used to calculate the nominal compositions, was not the appropriate one. The refined (Ca+Zn)/P ratios are close to the nominal value of 1.67. It seems that the Zn-incorporation in BCP is governed by the Ca/P ratio (instead of the (Ca+Zn)/P ratio): when this ratio decreases

dx.doi.org/10.1021/cm200537v |*Chem. Mater.* 2011, 23, 3072–3085

Table 4. Refinement Results (lattice parameters *a* and *c*; unit-cell volume *V*; atomic coordinates *x*, *y*, and *z*; temperature factors B_{iso}; and occupancies) on the Hydroxyapatite Phase in the Zn-Substituted Samples[a]

sample	HAp	atom	site	*x*	*y*	*z*	B_{iso} (Å^2)	occupancy
$Zn_{0.00}$-BCP	$Ca_{10}(PO_4)_6(OH)_2$	Ca1	4*f*	1/3	2/3	0.0013 (2)	0.29 (2)	1
	$P6_3/m$	Ca2	6*h*	0.2462 (1)	0.9926 (1)	1/4	$= B_{Ca1}$	1
	a = 9.4207 (1) Å	P1	6*h*	0.3988 (2)	0.3691 (2)	1/4	0.38 (3)	1
	c = 6.8817 (1) Å	O1	6*h*	0.3260 (3)	0.4830 (3)	1/4	0.12 (3)	1
	V = 528.93 (1) Å^3	O2	6*h*	0.5875 (3)	0.4653 (3)	1/4	$= B_{O1}$	1
	cR_p = 0.059	O3	12*i*	0.3407 (2)	0.2559 (2)	0.0704 (2)	$= B_{O1}$	1
	cR_{wp} = 0.071	OH4	4*e*	0	0	0.2030 (9)	$= B_{O1}$	1/2 (-)
	χ^2 = 3.45							
$Zn_{0.25}$-BCP	$Ca_{10}Zn_{0.25(1)}(PO_4)_6O_{0.50(2)}(OH)_{1.50(2)}$	Ca1	4*f*	1/3	2/3	0.0033 (3)	0.83 (2)	1
	$P6_3/m$	Ca2	6*h*	0.2468 (2)	0.9934 (2)	1/4	$= B_{Ca1}$	1
	a = 9.4112 (1) Å	P1	6*h*	0.3989 (2)	0.3692 (2)	1/4	0.54 (4)	1
	c = 6.9009 (1) Å	O1	6*h*	0.3270 (4)	0.4834 (4)	1/4	0.80 (4)	1
	V = 529.33 (1) Å^3	O2	6*h*	0.5862 (5)	0.4637 (5)	1/4	$= B_{O1}$	1
	cR_p = 0.089	O3	12*i*	0.3393 (3)	0.2537 (3)	0.0697 (4)	$= B_{O1}$	1
	cR_{wp} = 0.090	OH4	4*e*	0	0	0.206 (1)	$= B_{O1}$	1/2 (-)
	χ^2 = 4.16	Zn1	2*b*	0	0	0	$= B_{Ca1}$	0.126 (6)
$Zn_{0.50}$-BCP	$Ca_{10}Zn_{0.26(1)}(PO_4)_6O_{0.52(2)}(OH)_{1.48(2)}$	Ca1	4*f*	1/3	2/3	0.0018 (2)	0.77 (2)	1
	$P6_3/m$	Ca2	6*h*	0.2474 (1)	0.9938 (2)	1/4	$= B_{Ca1}$	1
	a = 9.4077 (1) Å	P1	6*h*	0.3986 (2)	0.3687 (2)	1/4	0.60 (3)	1
	c = 6.9077 (1) Å	O1	6*h*	0.3273 (4)	0.4826 (4)	1/4	0.77 (4)	1
	V = 529.46 (1) Å^3	O2	6*h*	0.5883 (4)	0.4651 (4)	1/4	$= B_{O1}$	1
	cR_p = 0.076	O3	12*i*	0.3406 (3)	0.2549 (3)	0.0691 (3)	$= B_{O1}$	1
	cR_{wp} = 0.081	OH4	4*e*	0	0	0.211 (1)	$= B_{O1}$	1/2(-)
	χ^2 = 4.46	Zn1	2*b*	0	0	0	$= B_{Ca1}$	0.132 (6)
$Zn_{0.50}$-BCP	*$Ca_{10}Zn_{0.3(1)}(PO_4)_6O_{0.7(1)}(OH)_{1.2(4)}$*	*Ca1*	*4f*	*1/3*	*2/3*	*0.0011 (5)*	*0.98 (4)*	*1*
	$P6_3/m$	*Ca2*	*6 h*	*0.2447 (4)*	*0.9921 (4)*	*1/4*	*$= B_{Ca1}$*	*1*
	a = 9.40822 (8) Å	*P1*	*6 h*	*0.3976 (3)*	*0.3675 (3)*	*1/4*	*0.54 (4)*	*1*
	c = 6.90756 (6) Å	*O1*	*6 h*	*0.3283 (3)*	*0.4850 (3)*	*1/4*	*1.24 (2)*	*1*
	V = 529.505 (8) Å^3	*O2*	*6 h*	*0.5886 (3)*	*0.4652 (3)*	*1/4*	*$= B_{O1}$*	*1*
	cR_p = 0.067, 0.072	*O3*	*12i*	*0.3442 (2)*	*0.2587 (2)*	*0.0709 (2)*	*$= B_{O1}$*	*1*
	cR_{wp} = 0.074, 0.080	*O4*	*4e*	*0*	*0*	*0.2075 (8)*	*$= B_{O1}$*	*0.480 (3)*
	χ^2 = 2.55	*H4*	*4e*	*0*	*0*	*0.05 (5)*	*$= 1.2xB_{O1}$*	*0.31 (9)*
		Zn1	*2b*	*0*	*0*	*0*	*$= B_{Ca1}$*	*0.15 (7)*
$Zn_{1.00}$-BCP	$Ca_{10}Zn_{0.12(1)}(PO_4)_6O_{0.24(2)}(OH)_{1.76(2)}$	Ca1	4*f*	1/3	2/3	0.0011 (6)	1.00 (5)	1
	$P6_3/m$	Ca2	6*h*	0.2486 (3)	0.9955 (4)	1/4	$= B_{Ca1}$	1
	a = 9.4142 (1) Å	P1	6*h*	0.4008 (4)	0.3707 (4)	1/4	0.43 (3)	1
	c = 6.8936 (1) Å	O1	6*h*	0.3255 (8)	0.4794 (9)	1/4	1.1 (1)	1
	V = 529.11 (1) Å^3	O2	6*h*	0.5864 (9)	0.4595 (9)	1/4	$= B_{O1}$	1
	cR_p = 0.069	O3	12*i*	0.3392 (6)	0.2512 (7)	0.0702 (8)	$= B_{O1}$	1
	cR_{wp} = 0.074	OH4	4*e*	0	0	0.203 (3)	$= B_{O1}$	1/2 (−)
	χ^2 = 3.87	Zn1	2*b*	0	0	0	$= B_{Ca1}$	0.060 (6)
$Zn_{0.25}Mg_{0.25}$-BCP	$Ca_{10}Zn_{0.25(1)}(PO_4)_6O_{0.50(2)}(OH)_{1.50(2)}$	Ca1	4*f*	1/3	2/3	0.0017 (3)	0.83 (2)	1
	$P6_3/m$	Ca2	6*h*	0.2470 (2)	0.9936 (2)	1/4	$= B_{Ca1}$	1
	a = 9.4153 (1) Å	P1	6*h*	0.3979 (2)	0.3679 (2)	1/4	0.49 (3)	1
	c = 6.8992 (1) Å	O1	6*h*	0.3280 (4)	0.4821 (4)	1/4	0.74 (4)	1
	V = 529.66 (1) Å^3	O2	6*h*	0.5877 (4)	0.4654 (5)	1/4	$= B_{O1}$	1
	cR_p = 0.079	O3	12*i*	0.3417 (3)	0.2554 (3)	0.0688 (4)	$= B_{O1}$	1
	cR_{wp} = 0.089	OH4	4*e*	0	0	0.213 (1)	$= B_{O1}$	1/2 (-)
	χ^2 = 5.58	Zn1	2*b*	0	0	0	$= B_{Ca1}$	0.126 (6)

dx.doi.org/10.1021/cm200537v |*Chem. Mater.* 2011, 23, 3072–3085

Table 4. Continued

sample	HAp	atom	site	x	y	z	B_{iso} (Å^2)	occupancy
$Zn_{0.25}Sr_{0.25}$-BCP	$Ca_{9.81(1)}Zn_{0.23(1)}Sr_{0.19(1)}(PO_4)_6O_{0.46(2)}(OH)_{1.54(2)}$	Ca1	4*f*	1/3	2/3	0.0022 (3)	0.87 (2)	1
	*P*6$_3$/*m*	Ca2	6*h*	0.2463 (2)	0.9932 (2)	1/4	= B_{Ca1}	0.968 (2)
	a = 9.4221 (1) Å	Sr2	6*h*	= x_{Ca2}	= y_{Ca2}	= z_{Ca2}	= B_{Ca1}	1-Occ$_{(Ca2)}$
	c = 6.9046 (1) Å	P1	6*h*	03982 (2)	0.3685 (2)	1/4	0.74 (4)	1
	V = 530.84 (1) Å^3	O1	6*h*	0.3292 (4)	0.4844 (4)	1/4	0.82 (4)	1
	cR_p = 0.097	O2	6*h*	0.5854 (4)	0.4644 (4)	1/4	= B_{O1}	1
	cR_{wp} = 0.091	O3	12*i*	0.3404 (3)	0.2555 (3)	0.0691 (3)	= B_{O1}	1
	χ^2 = 5.58	OH4	4*e*	0	0	0.208 (1)	= B_{O1}	1/2 (-)
		Zn1	2*b*	0	0	0	= B_{Ca1}	0.113 (6)

[a] Standard deviations are indicated in parentheses (accuracy can be estimated as being 3σ). cR_p and cR_{wp} represent conventional Rietveld agreement factors, and χ^2 is a goodness of fit indicator defined by $(R_{wp}/R_{exp})^2$ (with R_{exp} the expected weighted profile factor). Italic characters correspond to values extracted from Rietveld refinement from neutron patterns for $Zn_{0.50}$-BCP.

from 1.67 to 1.50 (from sample $Zn_{0.00}$-BCP to $Zn_{1.00}$-BCP) the HAp phase is replaced by the β-TCP phase, and when the ratio decreases below 1.50 (from sample $Zn_{1.00}$-BCP to $Zn_{2.00}$-BCP), ZnO is present with β-TCP. This observation indicates that incorporation of Zn cations into the HAp structure is not realized by Ca substitution.

Quantitative phase analyses from the cosubstituted samples are in agreement with our previous results on the alkaline-earth substitutions: small Mg^{2+} cations enter only weakly in the HAp structure in contrast to large Sr^{2+} cations, which preferentially substitute calcium in the Ca2 site in the HAp structure. Solid symbols in Figure 2, Zn−Mg cosubstituted sample, show the β-TCP stabilizing feature of Mg^{2+}, whereas crossed symbols indicate the incorporation of Sr^{2+} into HAp structure.

3.2. Zn Insertion into the HAp Structure. In the course of the refinements one additional crystallographic site has been considered in the HAp structure for Zn atoms. Site occupancies of both Ca1 and Ca2 sites in the HAp structure were refined extremely close to unity by considering calcium atoms only; indicating that heavy Zn atoms did not substitute calcium (in which case an occupancy superior to unity for Ca1 and/or Ca2 would have been refined). This result on Zn-HAp heat-treated at 1100 °C contrasts with previous results from Tang et al.[33] and Matsunaga et al.,[45] indicating the Zn substitution preferentially in the Ca2 site. Refinements also indicate 100% occupancy for the PO_4 tetrahedron. Difference Fourier maps have shown the existence of electron density on the 2*b* Wyckoff site at (0, 0, 0). Maps calculated from powder data are more diffuse than those calculated from single crystal data, but they are still quite usable for completing a structural model.[52] This electron density has been attributed to Zn atoms located in the new 2*b* site because such a supplementary electron density was never observed before (in our previous crystallochemical characterisations of undoped HAp, and of Mg-, Sr-, and Si-doped HAp phases[24−27]) and because Zn is the only additional element (reagents were $Ca(NO_3)_2.4H_2O$, $Zn(NO_3)_2.6H_2O$, and P_2O_5 only); nitrate if present in the as synthesized sample would have been evacuated during the heat treatment at 1100 °C (Raman spectroscopic have shown the absence of nitrate in the heat treated samples). Independent Rietveld refinements on XRPD and NPD patterns for $Zn_{0.50}$-BCP sample have shown not only the same mineralogical compositions (with equivalent weight percent, see Table 3), but also equivalent Zn populations in the 2*b* site: occupancie refined at 0.132(6) with XRPD and at 0.15(7) with NPD

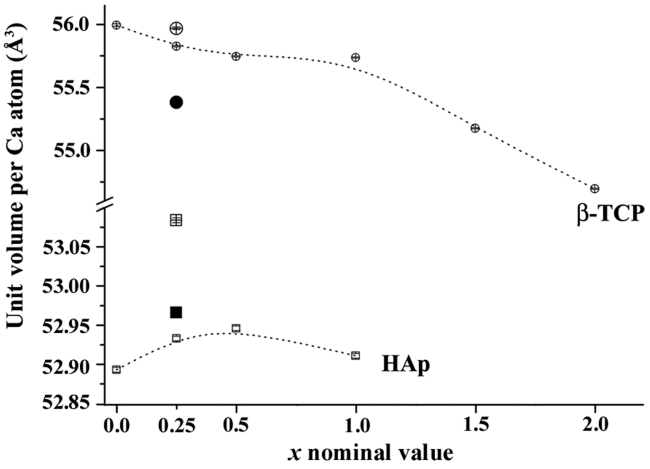

Figure 3. Variation in the unit volume per Ca atom for HAp (squares) and β-TCP (circles); i.e., the unit-cell volume divided by 10 for HAp, and by 63 for β-TCP. Co-substituted samples, Zn−Mg and Zn−Sr are represented by solid and crossed symbols respectively. Dotted lines are only guides for the eyes, and correspond to the single Zn-BCP series (without taking into account cosubstituted samples). Error bars are represented, but are within symbols.

(Table 4). Standard deviation on Zn occupancie is smaller with XRPD because Zn contrast is favorable for X-ray diffraction (Zn/Ca ratio of 1.5 for X-ray scattering factors, against 1.2 for bound coherent neutron scattering lenghts). Refining equivalent Zn population from XRPD (considering electronic density) and from NPD (considering nucleus population) strenghen the 2*b* site is actually partially occupied by Zn. SEM-EDS quantitative analyses on hydroxyapatite crystals have shown heterogeneous atomic Ca/Zn ratios centered around 40 (approximately between 30 and 60).

The evolution of the unit-cell volume of the HAp phase when introducing Zn^{2+} during the synthesis process does not evidence either a calcium substitution mechanism (see evolution of unit volume per calcium atom in Figure 3, i.e., unit-cell volume divided by 10). There is almost no variation—or a weak increase—in the unit-cell volume when introducing Zn (despite the smaller size of Zn^{2+} compared to Ca^{2+}, see Table 1, that would result in a decrease of the unit-cell volume). An observation of the lattice parameters of HAp shows opposite variation of basal *a* and axial *c* lattice parameters: when incorporating Zn

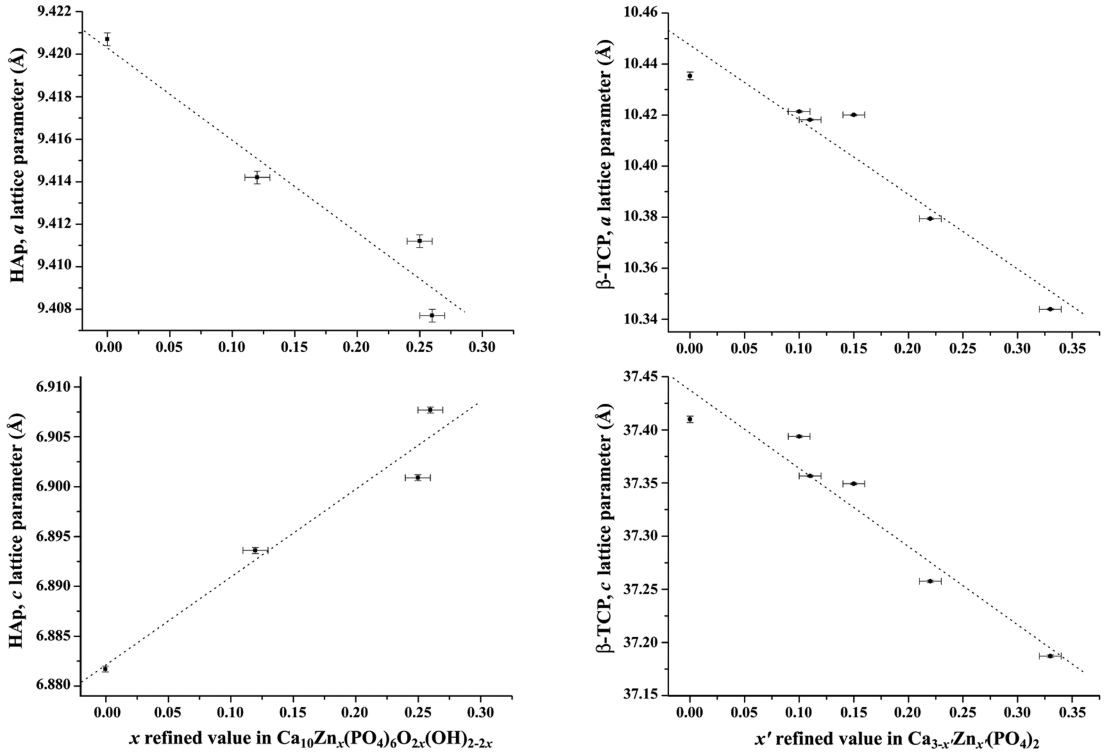

Figure 4. Variations in the lattice parameters *a* (top) and *c* (bottom) of the Zn-inserted HAp with $Ca_{10}Zn_x(PO_4)_3O_{2x}(OH)_{2-2x}$ composition (squares, right) and Zn-substituted β-TCP with $Ca_{3-x'}Zn_{x'}(PO_4)_2$ composition (circles, left). Error bars correspond to 3σ, with σ the standard deviations extracted from Rietveld treatments.

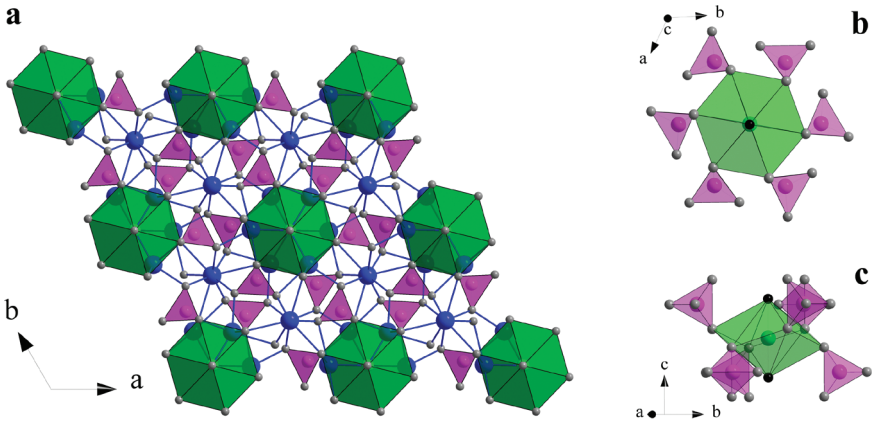

Figure 5. Representations of the Zn-substituted HAp structure. General view (a), environment of Zn^{2+} cation projected along [001] (b) and in (011) (c). Calcium atoms are represented by blue spheres (with bonding to oxygen in blue), oxygen atoms are represented by gray spheres, phosphate tetrahedra are represented by pink polyhedra and zinc polyhedra are represented by green polyhedra. Split O4 sites are ordered (to maintain acceptable Zn−O interatomic distance) and are represented with black spheres in Figure 5b and 5c.

into HAp, the *a* parameter decreases, whereas the *c* parameter increases (Figure 4 left). All the refined structural parameters for HAp phase are gathered in Table 4. The Zn insertion mechanism in HAp (in the 2*b* Wyckoff site) correlates with the unusual evolution of lattice parameters and explains the mineralogical evolution when introducing Zn (disappearence of HAp and stabilization of β-TCP). To maintain electroneutrality of the Zn-doped HAp phase, we have to consider proton vacancies to replace hydroxyl anions by O^{2-} around the 2*a* site. Then the general formula for Zn-incorporated HAp phase should be written $Ca_{10}Zn_x(PO_4)_6O_{2x}(OH)_{2-2x}$ with formation of linear O−Zn−O entities. Such an insertion of Zn in the 2*b* site corresponds to the formation of an insertion solid solution. Incorporated Zn^{2+} cations are excess cations for HAp with respect to the considered (Ca+Zn)/P ratio of 1.67 (using reagent ratio corresponding to a nominal composition of $Ca_{10-x}Zn_x(PO_4)_6(OH)_2$ by considering the usual substitution mechanism).

Zn atoms are located along the hexagonal axis, between two close oxygen atoms from the O4 site and six distant oxygen atoms from the O3 site (belonging to the phosphate group). The

dx.doi.org/10.1021/cm200537v |*Chem. Mater.* 2011, 23, 3072–3085

introduction of Zn^{2+} in the HAp hexagonal channel site organizes the local structure. O4 was convergently refined in a split position shifted along z by about 0.3 Å from the Ca2 triangle plane. The refined z coordinate of O4 represents a superposition of hydroxyl groups and oxygen O^{2-} anions coordinated to Zn. Thus real interatomic distance Zn−O4 lies most probably within maximum (2.02 Å) and minimum (1.40 Å) values to be physically reasonable. For 2-fold linearly coordinated Zn^{2+} cation, no reliable data has been found in the literature (contrary to Ni^{2+}, in K_2NiO_2,[61] with d_{Ni-O} = 1.68 Å). The Zn-inserted HAp structure is represented in Figure 5, in which the 2 + 6 coordination polyhedron (pseudohexagonal-based bipyramid) has been considered for Zn^{2+}. The 2*b* site can only be half-filled (considering isolated O−Zn−O entities), corresponding to the limit formula $Ca_{10}Zn_1(PO_4)_6O_2$ (complete replacement of hydroxyls by O^{2-} anions). The largest refined Zn proportion in our samples is $Ca_{10}Zn_{0.26(1)}(PO_4)_6O_{0.52(2)}(OH)_{1.48(2)}$ (for $Zn_{0.50}$-BCP sample, see Table 4). Zn atoms fill about 25% of the available 2*b* sites only. This relatively small proportion of inserted Zn cation could be explained either because electronic compensation (hydroxyl replacement by O^{2-}) is not easily realized (i.e., is destabilizing the HAp structure), or because large distortion of the neighboring phosphate tetrahedra. Zn atoms are 8-fold coordinated in their interstitial site. Nevertheless, due to the large differences in interatomic distances in the coordination polyhedron, it is more appropriate to indicate a 2 + 6 coordination with two Zn−O4 distances around 1.7 Å (considering O4 located in the average 2*a* site position) and six Zn−O3 distances around 2.9 Å. When filling a 2*b* site, the Zn cation pushes the two close hydroxyl anions (by locally blocking its splitting), and attracts the six far O3 oxygen anions. This is observable by the appearance of a distortion of the phosphate group. Whereas the PO_4 tetrahedron is almost regular in the unsubstituted HAp structure with four P−O distances about 1.54 Å (one P−O1 distance, one P−O2 distance and two P−O3 distances), it becomes elongated along the P−O3 direction when Zn is inserted in the HAp structure (distances P−O3 about 1.56 Å, and distances P−O1 and P−O2 about 1.53 Å, for $Zn_{0.25}$-BCP and $Zn_{0.50}$-BCP samples). The real PO_4 distortion around Zn is certainly more important than the one obtained by Rietveld treatment considering long-range ordering.

Concerning the cosubstituted samples, observations are in agreement with indications given by the single substituted samples. Zn^{2+} cations are inserted in the HAp structure in the proportion previously described. Large Sr^{2+} cations substitute for Ca^{2+} cations in the Ca2 site[24,25] and small Mg^{2+} cations are barely incorporated in the HAp structure,[26] explaining the β-TCP stabilizing feature of Mg^{2+}.

3.3. Zn Substitution in the β-TCP Phase. The Zn incorporation into the β-TCP structure follows a usual substitution mechanism as indicated in Figure 3. Unit-cell volume of β-TCP is decreasing when replacing Ca^{2+} by smaller Zn^{2+}. No straight variations are expected in Figure 3 (neither for β-TCP, nor for HAp) as abscise is the x nominal value and not the inserted Zn percentage in each phase. Figure 4 right shows Vegard's law by considering the refined x' value in the substitution solid solution described by the general formula $Ca_{3-x'}Zn_{x'}(PO_4)_2$. Zn^{2+} substitutes for Ca^{2+} in the calcium sites of the β-TCP structure. No additional specific site has been observed for Zn atoms in β-TCP; i.e. difference Fourier maps did not show new locations of electronic density. Lattice parameters, unit-cell volumes, Zn occupancies in the calcium substitution sites, and refined compositions of β-TCP are gathered in Table 5. Zn^{2+} substitutes for calcium cations only in the Ca4 and Ca5 sites: the calcium sites belonging to the low density column described by Yashima et al.[56] Our previous results have indicated a preference for the Ca5 site for substitution by small Mg^{2+} cations, whereas large

Table 5. Lattice Parameters, Unit-Cell Volumes, Zn Occupancies in the Calcium Substitution Sites (Ca3, Ca4, and Ca5), and Refined Compositions of the Zn-Substituted β-TCP Phase[a]

		Zn substitution		
sample	βΠXT	atom	site	occupancy
$Zn_{0.00}$-BCP	$Ca_3(PO_4)_2$			
	*R*3*c*			
	a = 10.4354 (5) Å			
	c = 37.396 (1) Å			
	V = 3526.8 (2) Å^3			
$Zn_{0.25}$-BCP	$Ca_{2.90(1)}Zn_{0.10(1)}(PO_4)_2$	Ca4	6*a*	0.15 (3)
	*R*3*c*	Zn4	6*a*	1/2-Occ$_{(Ca4)}$
	a = 10.4214 (1) Å			
	c = 37.3938 (4) Å			
	V = 3517.1 (1) Å^3			
$Zn_{0.50}$-BCP	$Ca_{2.85(1)}Zn_{0.15(1)}(PO_4)_2$	Ca4	6*a*	0.15 (2)
	*R*3*c*	Zn4	6*a*	1/2-Occ$_{(Ca4)}$
	a = 10.4201 (1) Å	Ca5	6*a*	0.84 (2)
	c = 37.3493 (3) Å	Zn5	6*a*	1-Occ$_{(Ca5)}$
	V = 3512.0 (1) Å^3			
$Zn_{1.00}$-BCP	$Ca_{2.89(1)}Zn_{0.11(1)}(PO_4)_2$	Ca4	6*a*	0.37 (1)
	*R*3*c*	Zn4	6*a*	1/2-Occ$_{(Ca4)}$
	a = 10.4182 (1) Å	Ca5	6*a*	0.75 (1)
	c = 37.3567 (3) Å	Zn5	6*a*	1-Occ$_{(Ca5)}$
	V = 3511.4 (1) Å^3			
$Zn_{1.50}$-BCP	$Ca_{2.78(1)}Zn_{0.22(1)}(PO_4)_2$	Ca4	6*a*	0.40 (1)
	*R*3*c*	Zn4	6*a*	1/2-Occ$_{(Ca4)}$
	a = 10.3794 (1) Å	Ca5	6*a*	0.33 (1)
	c = 37.2576 (4) Å	Zn5	6*a*	1-Occ$_{(Ca5)}$
	V = 3476.1 (1) Å^3			
$Zn_{2.00}$-BCP	$Ca_{2.67(1)}Zn_{0.33(1)}(PO_4)_2$	Ca4	6*a*	0.31 (1)
	*R*3*c*	Zn4	6*a*	1/2-Occ$_{(Ca4)}$
	a = 10.3439 (1) Å	Ca5	6*a*	0.03 (1)
	c = 37.1871 (4) Å	Zn5	6*a*	1-Occ$_{(Ca5)}$
	V = 3445.8 (1) Å^3			
$Zn_{0.25}Mg_{0.25}$-BCP	$Ca_{2.82(3)}Zn_{0.07(1)}$ $Mg_{0.11(2)}(PO_4)_2$	Ca3	18*b*	0.93 (2)
	*R*3*c*	Mg3	18*b*	1-Occ$_{(Ca3)}$
	a = 10.3919 (1) Å	Ca4	6*a*	0.26 (2)
	c = 37.3060 (4) Å	Zn4	6*a*	1/2-Occ$_{(Ca4)}$
	V = 3489.0 (1) Å^3	Ca5	6*a*	0.83 (3)
		Mg5	6*a*	1-Occ$_{(Ca5)}$
$Zn_{0.25}Sr_{0.25}$-BCP	$Ca_{2.75(3)}Sr_{0.25(2)}(PO_4)_2$	Ca3	18*b*	0.88 (3)
	*R*3*c*	Sr3	18*b*	1-Occ$_{(Ca3)}$
	a = 10.4366 (3) Å	Ca4	6*a*	0.0 (-)
	c = 37.379 (1) Å	Sr4	6*a*	1/2 (-)
	V = 3525.9 (2) Å^3			

[a] Standard deviations are indicated in parentheses (accuracy can be estimated as being 3σ).

dx.doi.org/10.1021/cm200537v |*Chem. Mater.* 2011, 23, 3072–3085

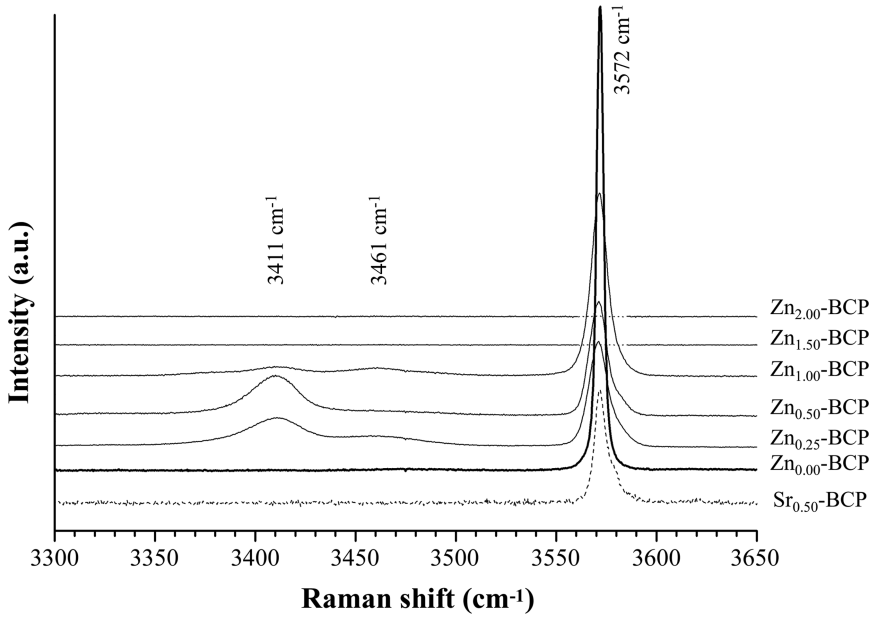

Figure 6. Raman spectra recorded from BCP samples in the spectral range 3300−3650 cm^{-1} corresponding to hydroxyl stretching. Normal, bold, and dotted lines correspond respectively to Zn-doped, undoped, and Sr-doped samples (Sr-containing sample is described in ref 24).

Sr^{2+} cations preferentially substitute the Ca4 site.[24−26] Recent study on the substitution mechanism of Zn ion in the β-TCP concludes to similar result with a substitution mechanism realized in the Ca5 site only.[62] The presence of large percentages of ZnO (up to 9 wt %) in the $Zn_{1.00}$-BCP, $Zn_{1.50}$-BCP and $Zn_{2.00}$-BCP samples indicates the limit of Zn-substitution in the β-TCP structure. A full occupancy of Ca4 and Ca5 sites (the low density column) by zinc leads to the composition $Ca_{2.57}Zn_{0.43}(PO_4)_2$.

Results from cosubstituted samples give interesting information. For the $Zn_{0.25}Mg_{0.25}$-BCP sample, each of the small cations is located in the same calcium crystallographic sites as those determined by studies on single substituted BCP. Mg^{2+} is mainly observed in the Ca5 site, but also in the Ca3 site, as mentioned in our previous study on the magnesium substitution in BCP,[26] and Zn^{2+} is observed in the Ca4 site (similar to the $Zn_{0.25}$-BCP sample). The $Zn_{0.25}Sr_{0.25}$-BCP case is somewhat different. Big Sr^{2+} cations are effectively localized in the site Ca4, i.e., the preferential crystallographic site determined in our previous study on strontium substitution in BCP.[24,25] Nevertheless, in the $Zn_{0.25}Sr_{0.25}$-BCP case, no Zn substitution was observed in β-TCP. It seems that the substitution of large atoms in the Ca4 site prevent the incorporation of small Zn^{2+} cations in the adjacent Ca5 site. Supplementary experimental results are needed to confirm this interpretation.

3.4. Raman Spectroscopy. Figure 6 shows the Raman spectra in the spectral range relative to hydroxyl stretching. Undoped BCP sample (bold line) presents a unique sharp peak at 3572 cm^{-1} in agreement with the unique OH^- environment in the HAp structure and the absence of OH^- in β-TCP. The observed band position corresponds with published values (IR spectroscopy[63] and Raman spectroscopy[64,65]). When introducing Zn in the samples, two new OH^- stretching broad bands are observed (see spectra from samples $Zn_{0.25}$-BCP, $Zn_{0.50}$-BCP and $Zn_{1.00}$-BCP) at 3411 and 3461 cm^{-1}. The signal at 3461 cm^{-1} appears for low Zn amount in HAp (spectrum from $Zn_{1.00}$-BCP sample containing an HAp phase with the $Ca_{10}Zn_{0.12(1)}(PO_4)_6O_{0.24(2)}(OH)_{1.76(2)}$ composition) and is replaced by the signal at 3411 cm^{-1} for higher Zn amount in HAp (spectra from $Zn_{0.50}$-BCP sample containing an HAp phase with the $Ca_{10}Zn_{0.26(1)}(PO_4)_6O_{0.52(2)}(OH)_{1.48(2)}$ composition). The total absence of vibrational signal in the 3300 − 3650 cm^{-1} spectral range for $Zn_{1.50}$-BCP and $Zn_{2.00}$-BCP samples corresponds with the absence of the HAp phase. The presence of new hydroxyl stretching bands in Zn-incorporated HAp evidence large modification in the hydroxyl environment. Such a large modification is not observed when introducing Sr into the HAp structure. The dotted line in Figure 6 corresponds to Raman spectra from a $Sr_{0.50}$-BCP sample, which contains HAp with the $Ca_{9.76(2)}Sr_{0.24(2)}(PO_4)_6(OH)_2$ composition, described in a previous study on strontium substitution in BCP.[24] The strontium incorporation into HAp structure, by a calcium substitution mechanism, induces only a broadening of the OH^- stretching band without displacement of the band and without appearance of new band of vibration. Presence of more electronegative cations in the OH^- vicinity induces the presence of new bands downshifted by some tens of cm^{-1}: 15, 30, and 50 cm^{-1}, respectively, when one, two, and three iron cations, respectively, substitute magnesium in the neighborhood of OH^- in nephrite.[66] The downshift of about 160 cm^{-1} obtained in Zn-inserted HAp correlates to the insertion mechanism with important modification on the OH^- environment. In pure HAp, oxygen atom from hydroxyl group (when located on the 2*a* Wyckoff site) has 3 neighboring Ca atoms (at about 2.4 Å), 6 neighboring O atoms (at about 3.2 Å) from 3 phosphate groups and 2 neighboring O atoms (at about 3.4 Å) from hydroxyl groups. Insertion of Zn^{2+} in site 2*b* with formation of O−Zn−O linear entities implies some OH^- groups are replaced by terminal oxygen from O−Zn−O. Then, the two new signals at 3461 and 3411 cm^{-1} should correspond to stretching of OH^- with replacement of, respectively, one and two neighboring OH^- groups by oxygen atom (from one or two O−Zn−O entities respectively).

Vibrational modes of phosphate tetrahedra were also investigated. The intense ν_1 internal mode, corresponding to symmetric stretching of the P−O bonds has been chosen here, namely

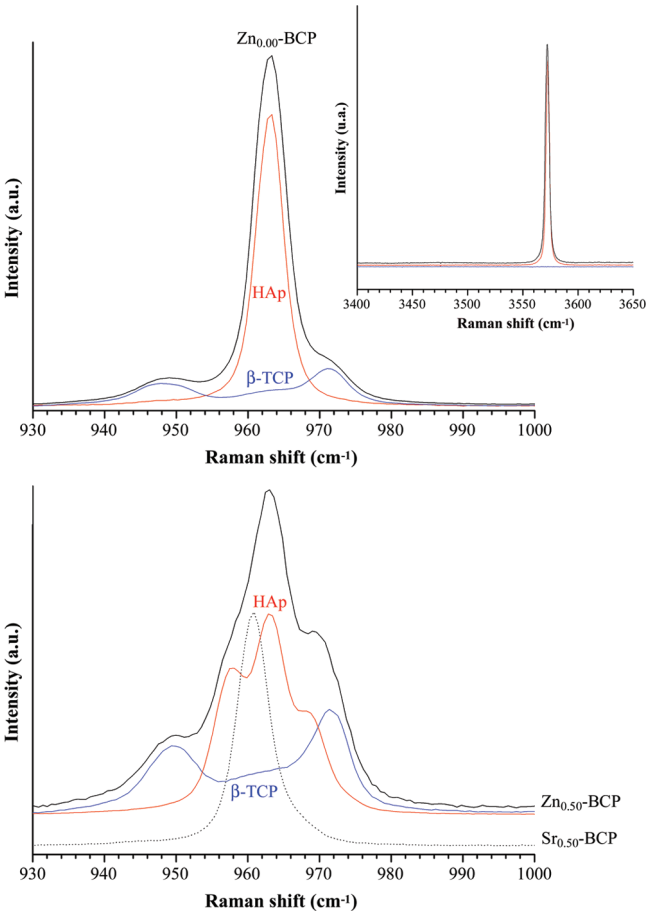

Figure 7. Raman spectra recorded from $Zn_{0.00}$-BCP sample (top), and $Zn_{0.50}$-BCP and $Sr_{0.50}$-BCP samples (bottom) in the spectral range 930−1000 cm^{-1}. Top: black line corresponds to the whole $Zn_{0.00}$-BCP sample (objective 10×), whereas red and blue lines, respectively, are related to HAp and β-TCP single domains (objective 100×). Inset relates the 3400−3650 cm^{-1} spectral range. Bottom: Raman spectra recorded from $Zn_{0.50}$-BCP (solid lines; whole BCP sample as well as single HAp and β-TCP domains) and $Sr_{0.50}$-BCP (dotted line, sample described in ref 24) samples in the spectral range 930−1000 cm^{-1}.

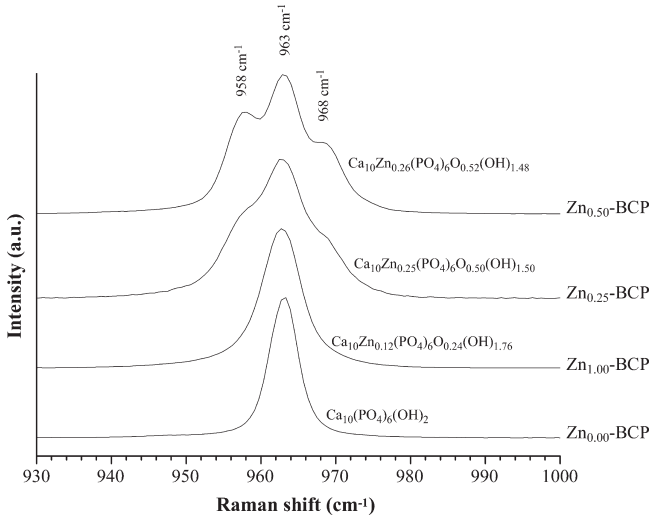

Figure 8. Raman spectra recorded from HAp single domains (objective x 100) from Zn_x-BCP samples with x = 0.00, 0.25, 0.50, and 1.00. Refined compositions (from Rietveld analyses, see Table 4) of the Zn-inserted HAp phase are indicated.

because it dominates the Raman spectra. Figure 7 (for $Zn_{0.00}$-BCP and $Zn_{0.50}$-BCP samples in the spectral ranges 930−1000 cm^{-1}, and 3300−3650 cm^{-1} for inset) shows how the micro-Raman can be used to easily differentiate the HAp and β-TCP phases: black lines relate the whole BCP samples (weak enlargements with the x10 objective) whereas red, respectively blue, lines relate the HAp, respectively β-TCP, single domains from BCP (large enlargements with the x100 objective). Whole BCP spectrum is exactly the combination of the two spectra from each single domain region. Inset in Figure 7 (spectral range relative to hydroxyl stretching) evidence the spectral attribution for HAp single phase region with OH^- vibration at 3572 cm^{-1} (red line), and for β-TCP single phase region without OH^- vibration (blue line). An intense peak—the ν_1 mode of vibration of $[PO_4]$—is observed at 963 cm^{-1} for HAp, whereas β-TCP presents several resolved signals with maxima at 948, 963, and 971 cm^{-1}; as already reported in the literature for both compounds.[64,63,67] Quillard et al.[68] have decomposed the spectra of β-TCP with five ν_1 bands at 946, 949, 959, 962, and 970 cm^{-1}, respectively, attributed to P1, P′1, P2, P′2, and P3 crystallographic sites (P′1 and P′2 refer to P1 and P2 sites, respectively, when the half-occupied Ca4 calcium site is empty). Because of large overlaps of the P1−P′1 and P2−P′2 doublets we have consider here only three distinct signals attributed to P1 (at 948 cm^{-1}), P2 (at 963 cm^{-1}), and P3 (at 971 cm^{-1}) according to ref 68. The incorporation of Zn into HAp leads to a highly deformed ν_1 signal (Figures 7 and 8). The intense single peak (assigned to the two A and E_2 symmetries combination,[69] whereas three Raman active components with A, E_1, and E_2 symmetries are expected from the correlation method[70]) is transformed in three resolved signals: the unchanged band at 963 cm^{-1} corresponding to phosphate groups unaffected by the Zn^{2+} incorporation and two new signals at 958 and 968 cm^{-1} corresponding to distorted phosphate tetrahedra. Such a modification in the ν_1 signal raised from the insertion mechanism for Zn^{2+}, contrary to the Sr^{2+} substitution mechanism which involved a downshift only (see spectra from Sr-substituted sample, dotted line in Figure 7 bottom). The band position at 960 cm^{-1} for $Ca_{9.76(2)}Sr_{0.24(2)}(PO_4)_6(OH)_2$ (from $Sr_{0.50}$-BCP sample[24]) agrees fairly well with the recent study of O'Donnell et al. indicating a linear decrease of the ν_1 band frequency with Sr-substitution (959 cm^{-1} was calculated for $Ca_{9.76}Sr_{0.24}(PO_4)_6(OH)_2$).[71] The significant shifts observed for the two new ν_1 signals (±5 cm^{-1}) correlate with the insertion mechanism which induces a local structure ordering. It assumed an important distortion of the phosphate tetrahedron in the vicinity of electronegative Zn. Evolution of the three ν_1 components in β-TCP when incorporating Zn^{2+} is represented in Figure 9, and band positions (obtained by spectral decomposition using three Lorentzian bands) are indicated in Table 6. The three ν_1 bands have different behaviors when increasing the Zn-substitution level: P1 signal is largely upshifted, P2 signal is downshifted for Zn_x-BCP with $x \geq 1.5$ only, and P3 signal is weakly upshifted. Phosphate groups relative to P1 site are directly concerned by the calcium substitution because they are bonded to Ca4 only (the unusual calcium site from the low density structural column[56]), whereas phosphate groups relative to P2 and P3 site are also bonded to the unsubstituted Ca1, Ca2 and Ca3 sites (from the high density structural column[56]). The position of

dx.doi.org/10.1021/cm200537v |Chem. Mater. 2011, 23, 3072–3085

the band relative to P2 site was unchanged for samples Zn_x-BCP with $0.00 \geq x \geq 1.0$ and was shifted down to 960 cm^{-1} for samples with $x \geq 1.5$. The geometrical characteristics of phosphate groups relative to P2 site are modified when Zn^{2+} hightly substitutes the neighbor Ca5 site: 67 and 97% for $Zn_{1.50}$-BCP and $Zn_{2.00}$-BCP, respectively (Table 6).

3.5. Microstructural Effect of Zn. A decrease in crystallinity has generally been associated with the incorporation of Zn in calcium phosphate.[42−44] In our study such behavior is not observed. Whatever the proportion of Zn, the refined microstructural parameters are always of the same order: coherent domain size about 900 Å for HAp and about 800 Å for β-TCP, and average maximal strain about 0.5 ‰ for HAp and about 1.0 ‰ for β-TCP. Nevertheless, our samples have been heat-treated at 1100 °C for 15 h in order to improve their crystallinity to allow reliable Rietveld refinements. Such a heat treatment is of great importance to describe in detail the crystallographic structure of the substituted powders, but evidently can suppress interesting intrinsic microstructural features of the as-precipitated powder.

4-. DISCUSSION

Structure refinement on the HAp phase have shown that Zn atoms do not substitute Ca atoms in Ca1 or Ca2 sites, but are located in the interstitial 2*b* Wyckoff site with coordinates (0, 0, 0) (see structural representation in Figure 5a). Small Zn^{2+} cations enter the hexagonal channel from the HAp structure. They occupy an 8-fold coordinated interstitial site with two short Zn−O4 distances (about 1.7 Å) and six long Zn−O3 distances (about 2.9 Å). The pseudohexagonal-based bipyramid is represented in panels b and c in Figure 5. When a Zn^{2+} cation is located in site 2*b*, it pushes on both sides the two close O4 atoms (the split hydroxyl anions) along the hexagonal axis, explaining the increase of the lattice parameter *c* (Table 4 and Figure 4). On the other side, Zn^{2+} attracts the six distant O3 atoms (belonging to the phosphate group that becomes elongated) in the basal plane; explaining the distortion of the phosphate tetrahedron (observed by Raman spectroscopy) and the decrease in the lattice parameter *a* (Table 4, Figure 4). The resulting moderate change in unit-cell volume (i.e., weak increase of the unit-cell volume when introducing small Zn^{2+} cations) confirms further the insertion mechanism of Zn atoms for HAp. Calculation of the bond valence sum, BVS,[72] of Zn^{2+} cation give a value of 2.2 when considering the eight neighbor oxygen atoms, and a value of 2.0 when considering the two close O4 oxygen atoms only. Average crystallographic structure does not describe accurately the local environment of Zn^{2+}: the apparent coordinate of O4 can still represent a superposition of oxygen atoms in the OH groups, oxygen atoms coordinated to Zn, and also lonely oxygen atoms. Thus real Zn−O4 distance can not be determined accurately, nevertheless an interatomic d_{Zn-O} distance of 1.7 Å seems acceptable according to BVS calculation and in comparison with published linearly coordinated Ni^{2+} cations[61,73,74] (no reliable data was founded for Zn^{2+} in the literature). The real Zn−O3 distances are expected to be shorter than the refined distances. The previously described distortion of the phosphate tetrahedron is actually more pronounced around Zn^{2+} cations, and can explain the apparently small proportion of Zn^{2+} inserted (occupancy about 1/8 only). This 2 + 6 coordination in an interstitial crystallographic site for zinc in HAp disagrees with recent spectroscopic results performed on comparable materials. Tang et al. have deduced from theoretical modeling and X-ray absorption spectroscopy that Zn favors the Ca2 site in tetrahedral coordination.[33] Matsunaga et al., according to first principles total energy calculations and X-ray absorption spectroscopy, concluded that the Zn^{2+} substitution is realized by a vacancy-filling mechanism in Ca-deficient HAp.[45] The present Rietveld analyses refutes such structural models with calcium substitution for Zn-HAp heat-treated at 1100 °C (calcium occupancy parameters were refined at unity for both Ca1 and Ca2 sites). Bazin et al. have localized Zn atoms, tetrahedrally coordinated, at the surface of pathological apatite.[46] Such physisorbed Zn species can not be checked by the present long-range order study. Nevertheless synthesis conditions should be considered

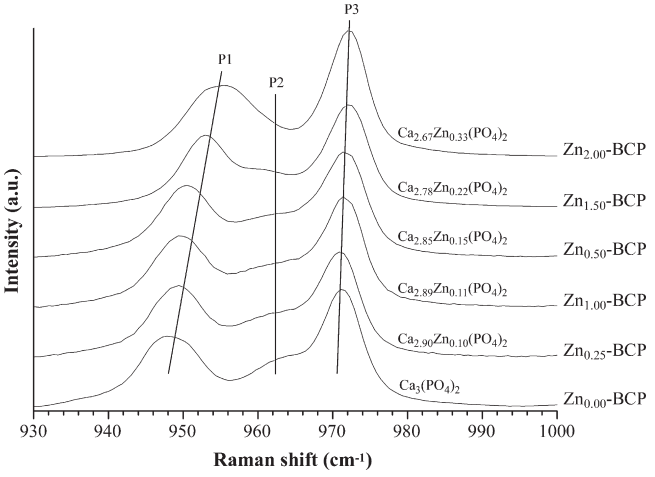

Figure 9. Raman spectra recorded from β-TCP single domains (objective x 100) from Zn_x-BCP samples with x = 0.00, 0.25, 0.50, 1.00, 1.50, and 2.00. Refined compositions (from Rietveld analyses, see Table 5) of the Zn-inserted β-TCP phase are indicated. Labels P1, P2, and P3 refer to the three phosphorus crystallographic sites.[68].

Table 6. Raman Shifts of the Three Independent Phosphate Tetrahedra in the β-TCP Structure Relative to the Three Phosphorus P1, P2, and P3 Crystallographic Sites with Indication of the Zn-Substitution Percentage in Ca4 and Ca5 Sites

		Zn substitution (%)		Raman shift (cm^{-1})		
sample	β-TCP refined composition	Ca4	Ca5	P1	P2	P3
$Zn_{0.00}$-BCP	$Ca_3(PO_4)_2$	0	0	948	963	971
$Zn_{0.25}$-BCP	$Ca_{2.90}Zn_{0.10}(PO_4)_2$	70	0	949	963	971
$Zn_{1.00}$-BCP	$Ca_{2.89}Zn_{0.11}(PO_4)_2$	26	25	949	963	971
$Zn_{0.50}$-BCP	$Ca_{2.85}Zn_{0.15}(PO_4)_2$	70	16	950	963	972
$Zn_{1.50}$-BCP	$Ca_{2.78}Zn_{0.22}(PO_4)_2$	20	67	953	961	972
$Zn_{2.00}$-BCP	$Ca_{2.67}Zn_{0.33}(PO_4)_2$	38	97	955	960	972

dx.doi.org/10.1021/cm200537v |*Chem. Mater.* 2011, 23, 3072–3085

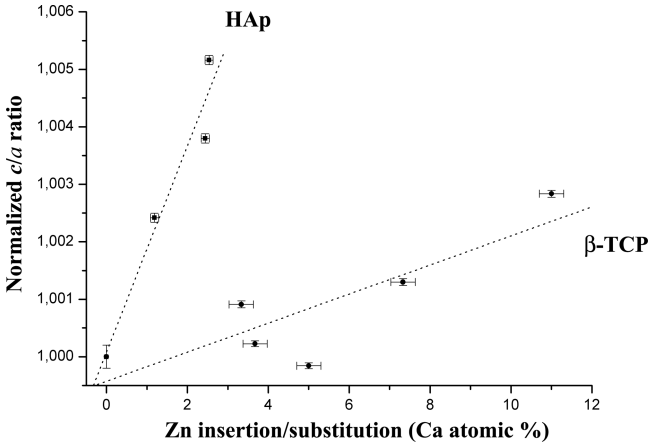

Figure 10. Variation of the normalized c/a ratios (i.e., $[c/a]/[c_0/a_0]$ with a_0 and c_0 the lattice parameters of the undoped phosphate phases) for HAp (squares) and β-TCP (circles). Error bars correspond to standard deviations extracted from Rietveld treatments (unsing 3σ for a and c lattice parameters). Dotted lines are only guides for the eyes.

before comparing the different results. Our samples have been heat-treated at 1100 °C for crystallinity reason. Temperature effect on the Zn incorporation in HAp will be described in a forthcoming paper.

Despite the almost equal ionic radii for Zn^{2+} and Mg^{2+} (Table 1), magnesium has not been observed in this interstitial site.[26] The different behavior between small 3d-metal Zn^{2+} and small alkaline-earth Mg^{2+} cations may be attributed to their highly different electronic structure and electronegativity. According to our knowledge, this is the first time that the Zn atom is located in the 2*b* site of the HAp structure. However, other 3d-metal ions have already been located in this interstitial site in apatite-like structures. This is namely the case for Cu^{2+}: Karpov et al. have refined from single crystal data the structure of $Ca_{10}Cu_{0.54}(PO_4)_6O_{1.72}H_y$ with Cu atoms in site 2*b*.[75] It corresponds to the same structure as our Zn-inserted HAp phase with a higher proportion of inserted Cu^{2+} (refined occupancy of 0.27, about twice of our occupancy of 0.13 for Zn^{2+}, see Table 4). The three 3d-metal ions Zn^{2+}, Ni^{2+}, and Co^{2+} have been also located in the same interstitial crystallographic site in belovite, the Sr-equivalent $Sr_{10}(PO_4)_6(OH)_2$ compound.[73]

The insertion of bivalent Zn^{2+} cation in hydroxyapatite induces the replacement of the hydroxyl anion by O^{2-} for electroneutrality reasons: $Ca_{10}Zn_x(PO_4)_6O_{2x}(OH)_{2-2x}$. According to this chemical formula, the proper ratio to consider for the preparation of single-phase sample is Ca/P = 1.67, and not (Ca+Zn)/P = 1.67. For this reason, the precipitation of β-TCP occurred when introducing Zn^{2+}. This (Ca+Zn)/P ratio has been frequently reported in the literature, and is at the origin of the reported inhibiting effect of zinc on HAp crystallization and the preference of Zn for β-TCP.[19,40,43,44,60] In spite of their nearly equal ionic radii, small Mg^{2+} and Zn^{2+} cations present different behavior with respect to HAp. Mg^{2+} has an inhibiting effect on the crystallization of HAp because its substitution for calcium is extremely limited, and its presence favors the formation of β-TCP; this contrasts with Zn^{2+}, which enters the HAp structure without substituting for calcium.

Zn^{2+} is also incorporated in the β-TCP structure, in which it substitutes for calcium cations leading to the general formula $Ca_{3-x'}Zn_{x'}(PO_4)_2$. The substitution process of zinc atoms for calcium is confirmed by the change of β-TCP unit-cell volume. Contrary to the HAp case, the unit-cell volume of β-TCP, as well as lattice parameters a and c, decreases when introducing small Zn^{2+} cations (Tables 4 and 5 and Figure 4). The evolution of the normalized c/a ratios (i.e., $[c/a]/[c_0/a_0]$ with a_0 and c_0 being the lattice parameters of the unsubstituted phosphate phases) represented in Figure 10 illustrates the anisotropic insertion mechanism observed for HAp, contrary to the relatively isotropic substitution mechanism for β-TCP. In the β-TCP case, there is a similarity with the behavior of small Mg^{2+} cations. Zn^{2+} inserts into the Ca5 site (similarly with Mg^{2+}), but also into the Ca4 site. The effect of cosubstitution, Zn−Mg and Zn−Sr, has brought interesting results. It seems possible to coinsert β-TCP with the two small doping elements Zn and Mg, whereas the incorporation of large Sr dopant excludes the simultaneous presence of Zn.

5-. CONCLUSION

The crystallographic study of eight well-crystallized Zn-substituted BCP samples (six single doped samples and two codoped samples with Mg and Sr heat-teated at 1100 °C) have brought new important information on the structural location of Zn^{2+} cation in both HAp and β-TCP phases. Rietveld refinement of XRPD patterns is a useful tool to reach a fine description of well-crystallized substituted materials. Rietveld refinement on powder patterns allows one to generate electronic density maps within the unit cell. This is a direct method to locate the substitution elements when allowed by the electronic contrast. Additional Rietveld refinement from NPD patterns and local information brought by Raman spectroscopy allows confirming structural details.

Zn^{2+} is incorporated in the β-TCP structure by substituting calcium atoms in the low-density column (i.e., in Ca4 and Ca5 crystallographic sites). Zn^{2+} enters the HAp structure and is located on the 2*b* Wyckoff site. Zn atoms do not substitute Ca atoms in Ca1 or Ca2 sites, but insert an interstitial site leading to the general formula $Ca_{10}Zn_x(PO_4)_6O_{2x}(OH)_{2-2x}$. Zn atoms are unusually 2 + 6 coordinated in HAp (with two short Zn−O distances of about 1.7 Å leading to the formation of linear O−Zn−O groups), contrary to recent spectroscopic interpretations that have indicated a tetrahedral configuration for Zn atoms located in calcium sites.[33,45] Such an insertion process induces an excess of cations, compensated by the replacement of hydroxyls by O^{2-} anions (forming the O−Zn−O group). These inserted Zn^{2+} cations are managed by the Ca/P ratio (of 1.67 with a nominal $Ca_{10}Zn_x(PO_4)_6O_{2x}(OH)_{2-2x}$ composition) instead of (Ca+Zn)/P ratio (with nominal $Ca_{10-x}Zn_x(PO_4)_6(OH)_2$ composition when considering usual substitution mechanism). The previously reported inhibiting effect of zinc on HAp crystallization, or destabilizing feature of zinc for HAp, is not inevitably intrinsic to Zn, but could be due to the nominal constituent ratio as clearly demonstrated here. These results pertain to sample that were annealed at high temperature, so the as-precipitated, less crystalline samples may be quite different. Careful examination of structural features involved by ionic substitution in calcium phosphate is absolutely needed to fully understand biological behavior of such ceramics.

AUTHOR INFORMATION

Corresponding Author

*E-mail: guillaume.renaudin@ensccf.fr. Tel.: 00 33 4 73 40 73 36. Fax.: 00 33 4 73 40 70 95.

■ ACKNOWLEDGMENT

This work was supported by ANR under project NANOSHAP (ANR-09-BLAN-0120-03). This work is partially based on the experiments carried out at the Swiss spallation neutron source SINQ at the Paul Scherrer Intitut, Villigen, Switzerland.

■ REFERENCES

(1) Dahl, S. G.; Allain, P.; Marie, P. J.; Mauras, Y.; Boivin, G.; Ammann, P.; Tsouderos, Y.; Delmas, P. D.; Christiansen, C. *Bone* **2001**, *28*, 446–453.
(2) Lagier, R.; Baud, C. A. *Pathol. Res. Pract.* **2003**, *199* (5), 329–335.
(3) Lee, R. S.; Kayser, M. V.; Ali, S. Y. *J. Anat.* **2006**, *208* (1), 13–19.
(4) Elliot, J.C., in *Structure and chemistry of the apatites and other calcium orthophosphates*, Amsterdam: Elsevier; 1994.
(5) Yao, F.; LeGeros, J. P.; LeGeros, R. Z. *Acta Biomater.* **2009**, *5*, 2169–2177.
(6) Kannan, S.; Goetz-Neunhoeffer, F.; Neubauer, J.; Pina, S.; Torres, P. M. C.; Ferreira, J. M. F. *Acta Biomater.* **2010**, *6*, 571–576.
(7) Blumenthal, N. C.; Betts, F.; Posner, A. S. *Calcif. Tissue. Inter.* **1975**, *18* (1), 81–90.
(8) Bigi, A; Cojazzi, G.; Panzavolta, S.; Ripamonti, A.; Roveri, N.; Romanello, M.; Noris Suarez, K.; Moro, L. *J. Inorg. Biochem.* **1997**, *68*, 45–51.
(9) Solomons, C. C.; Neuman, W. F. *J. Biol. Chem.* **1960**, *235*, 2502–2506.
(10) Bazin, D.; Carpentier, X.; Traxer, O.; Thiaudiere, D.; Somogyi, A.; Reguer, S.; Waychunas, G.; Jungers, P.; Daudon, M. *J. Synchrotron Radiat.* **2008**, *15*, 506–509.
(11) Murray, E. J.; Messer, H. H. *J. Nutr.* **1991**, *111*, 1641–1647.
(12) Bazin, D.; Chevallier, P.; Matzen, G.; Jungers, P.; Daudon, M. *Urol. Res.* **2007**, *35*, 179–184.
(13) Ito, A.; Otsuka, M.; Kawamura, H.; Ikeuchi, M.; Ohgushi, H.; Sogo, Y.; Ichinose, N. *Curr. Appl. Phys.* **2005**, *5*, 402–406.
(14) Yamaguchi, M.; Oishi, H.; Suketa, Y. *Biochem. Pharmacol.* **1987**, *36* (22), 4007–4012.
(15) Yamaguchi, M.; Yamaguchi, R. *Biochem. Pharmacol.* **1986**, *35* (5), 773–777.
(16) Wang, X.; Ito, A.; Sogo, Y.; Li, X.; Oyane, A. *Acta Biomater.* **2010**, *6*, 962–968.
(17) Ito, A.; Kawamura, H.; Otsuka, M.; Ikeuchi, M.; Ohgushi, H.; Ishikawa, K. *Mater. Sci. Eng.* **2002**, *C22*, 21–25.
(18) Ito, A.; Ojima, K.; Naito, H.; Ichinose, N.; Tateishi, T. *J. Biomed. Mater. Res.* **2000**, *50*, 178–183.
(19) Sogo, Y.; Ito, A.; Fukasawa, K.; Sakurai, T.; Ichinose, N. *Mater. Sci. Technol.* **2004**, *20* (9), 1079–1083.
(20) Jallot, E.; Nedelec, J. M.; Grimault, A. S.; Chassot, E.; Grandjean-Laqueriere, A.; Laquerriere, P.; Laurent-Maquin, D. *Colloids Surf., B* **2005**, *42*, 205–210.
(21) Velard, F.; Laurent-Maquin, D.; Braux, J.; Guillaume, C.; Bouthors, S.; Jallot, E.; Nedelec, J. M.; Belaaouaj, A.; Laquerriere, P. *Biomaterials* **2010**, *31*, 2001–2009.
(22) Grandjean-Laquerriere, A.; Laquerriere, P.; Jallot, E.; Nedelec, J. M.; Guenounou, M.; Laurent-Maquin, D.; Philips, T. M. *Biomaterials* **2006**, *27*, 3195–3200.
(23) Dong Li, J.; Bao Li, Y.; Zuo, Y.; Guo Yu Lv, G.; Wei Hu, Y.; Zhi Yue, T. *Mater. Sci. Forum* **2006**, *510−511*, 890–893.
(24) Renaudin, G.; Laquerriere, P.; Filinchuk, Y.; Jallot, E.; Nedelec, J. M. *J. Mater. Chem.* **2008**, *18* (30), 3593–3600.
(25) Renaudin, G.; Jallot, E.; Nedelec, J. M. *J. Sol−Gel Sci. Technol.* **2009**, *51* (3), 287–294.
(26) Gomes, S.; Renaudin, G.; Jallot, E.; Nedelec, J. M. *Appl. Mater. Interfaces* **2009**, *1* (2), 505–513.
(27) Gomes, S.; Renaudin, G.; Mesbah, A.; Jallot, E.; Bonhomme, C.; Babonneau, F.; Nedelec, J. M. *Acta Biomater.* **2010**, *6*, 3264–3274.
(28) Shannon, R. D. *Acta Crystallogr., Sect. A* **1976**, *A32*, 751–767.
(29) Bigi, A.; Foresti, E.; Gandolfi, M.; Gazzano, M.; Roveri, N. *J. Inorg. Biochem.* **1997**, *66* (4), 259–265.
(30) Suzuki, S.; Toshifumi, F.; Toru, M.; Minoru, T.; Yasuo, H. *J. Am. Ceram. Soc.* **1993**, *76* (6), 1638–1640.
(31) Kim, T. N.; Feng, Q. L.; Kim, J. O.; Wu, J.; Wang, H.; Chen, G. C. *J. Mater. Sci. Mater. Med.* **1998**, *9* (3), 129–134.
(32) Bruckner, S.; Lusvardi, G.; Menabue, L.; Saladini, M. *J. Mater. Chem.* **1993**, *3* (7), 715–719.
(33) Tang, Y.; Chappell, H. F.; Dove, M. T.; Reeder, R. J.; Lee, Y. J. *Biomaterials* **2009**, *30* (15), 2864–2872.
(34) Barrea, R. A.; Pérez, C. A.; Ramos, A. Y. *J. Synchroton Radiat.* **2001**, *8*, 990–992.
(35) Lang, J. *Bull. Soc. Sci. Bretagne* **1981**, *53*, 95–124.
(36) Cabrera, W. E.; Schrooten, I.; De Broe, M. E.; D'haese, P. C. *J. Bone Miner. Res.* **1999**, *14*, 661–668.
(37) Barrea, R. A.; Pérez, C. A.; Ramos, A. Y.; Sanchez, H. J.; Grenon, M. *X-Ray Spectrom.* **2003**, *32*, 387–395.
(38) Takatsuka, T.; Hirano, J.; Matsumoto, H.; Honma, T. *Eur. J. Oral Sci.* **2005**, *113*, 80–183.
(39) Zhu, K.; Yanagisawa, K.; Shimanouchi, R.; Onda, A.; Kaiyoshi, K. *J. Eur. Ceram. Soc.* **2006**, *26*, 509–513.
(40) Miyaji, F.; Kono, Y.; Suyama, Y. *Mater. Res. Bull.* **2005**, *40* (2), 209–220.
(41) Patel, P. N. *J. Inorg. Nucl. Chem.* **1980**, *42* (8), 1129–1132.
(42) Bigi, A.; Foresti, E.; Gandolfi, M.; Gazzano, M.; Roveri, N. *J. Inorg. Biochem.* **1995**, *58* (1), 49–58.
(43) Ren, F.; Xin, R.; Ge, X.; Leng, Y. *Acta Biomater.* **2009**, *5* (8), 3141–3149.
(44) Li, M. O.; Xiao, X.; Liu, R.; Chen, C.; Huang, L. *J. Mater. Sci.: Mater. Med.* **2008**, *19* (2), 797–803.
(45) Matsunaga, K.; Murata, H.; Mizoguchi, T.; Nakahira, A. *Acta Biomater.* **2010**, *6* (6), 2289–2293.
(46) Bazin, D.; Carpentier, X.; Brocheriou, I.; Dorfmuller, P.; Aubert, S.; Chappard, C. *Biochimie* **2009**, *91* (10), 1294–1300.
(47) Terra, J.; Jiang, M.; Ellis, D. E. *Philos. Mag., A* **2002**, *82* (11), 2357–2377.
(48) Ma, X.; Ellis, D. E. *Biomaterials* **2008**, *29* (3), 257–265.
(49) Matsunaga, K. *J. Chem. Phys.* **2008**, *128* (24), 245101–245110.
(50) Fischer, P.; Frey, G.; Koch, M.; Könnecke, M.; Pomjakushin, V.; Schefer, J.; Thut, R.; Schlumpf, N.; Bürge, R.; Greuter, U.; Bondt, S.; Berruyer, E. *Physica B* **2000**, *276*, 146–148.
(51) Rodriguez-Carvajal, J. *PROGRAM FullProf.2k — version 3.20*; Laboratoire Léon Brillouin (CEA-CNRS): Saclay, France, 2005; FullProf.2k manual available on http://www-llb.cea.fr/fullweb/fp2k/fp2k_divers.htm. See also J. Rodriguez-Carvajal, Roisnel, T.*EPDIC-8*; May 23−26 ,2002; Trans Tech Publication: Uppsala, Sweden; *Mater. Sci. Forum* 2004, 123, 443.
(52) McCusker, L. B.; Von Dreele, R. B.; Cox, D. E.; Louër, D.; Scardi, P. *J. Appl. Crystallogr.* **1999**, *32*, 36–50.
(53) Hill, R. J. *J. Appl. Crystallogr.* **1992**, *25*, 589–610.
(54) Hill, R. J.; Cranswick, L. M. D. *J. Appl. Crystallogr.* **1992**, *25*, 589–610.
(55) Rodriguez-Lorenzo, L. M.; Hart, J. N.; Gross, A. *J. Phys. Chem. B* **2003**, *107* (33), 8316–8320.
(56) Yashima, M.; Sakai, A.; Kamiyama, T.; Hoshikawa, A. *J. Solid State Chem.* **2003**, *175* (2), 272–277.
(57) Abrahams, S. C.; Bernstein, J. L. *Acta Crystallogr., Sect. B* **1969**, *B25*, 1233–1236.
(58) Madsen, I. C.; Scarlett, N. V. Y.; Cranswick, L. M. D.; Lwin, T. *J. Appl. Crystallogr.* **2001**, *34*, 409–426.
(59) Scarlett, N. V. Y.; Madsen, I. C.; Cranswick, L. M. D.; Lwin, T.; Groleau, E.; Stephenson, G.; Aylmore, M.; Agron-Olshina, N. *J. Appl. Crystallogr.* **2002**, *35*, 383–400.
(60) Sogo, Y.; Ito, A.; Fukasawa, K.; Sakurai, T.; Ichinose, N.; LeGeros, R. Z. *Key Eng. Mater.* **2005**, *284−286*, 31–34.
(61) Rieck, H.; Hoppe, R. *Z. Anorg. allg. Chem.* **1973**, *400*, 311–320.
(62) Kawabata, K.; Yamamoto, T.; Kitada, A. *Physica B* **2011**, *406* (4), 890–894.

(63) Fowler, B. O. *Inorg. Chem.* **1974**, *13* (1), 195–207.
(64) Cuscó, R.; Guitián, F.; De Aza, S.; Artús, L. *J. Eur. Ceram. Soc.* **1998**, *18*, 1301–1305.
(65) Zou, S.; Huang, J.; Best, S.; Bonfield, W. *J. Mater. Sci. Mater. Med.* **2005**, *16*, 1143–1148.
(66) Chen, T.-H.; Calligaro, T.; Pagès-Camagna, S.; Menu, M. *Appl. Phys. A: Mater. Sci. Process.* **2004**, *79*, 177–180.
(67) de Aza, P. N.; Santos, C.; Pazo, A.; De Aza, S.; Cuscó, R.; Artús, L. *Chem. Mater.* **1997**, *9*, 912–915.
(68) Quillard, S.; Paris, M.; Deniard, P.; Gildenhaar, R.; Berger, G.; Obadia, L.; Bouler, J.-M. *Acta Biomater.* **2011**, *7* (4), 1844–52.
(69) Tsuda, H.; Arends, J. *J. Dent. Res.* **1994**, *73*, 1703–1710.
(70) Nelson, D. G. A.; Williamson, B. E. *Aust. J. Chem.* **1982**, *35*, 715–727.
(71) O'Donnell, M. D.; Fredholm, Y.; de Rouffignac, A.; Hill, R. G. *Acta Biomater.* **2008**, *4*, 1455–1464.
(72) Brese, N. E. *Acta Crystallogr., Sect. B* **1991**, *B47*, 192–197.
(73) Kazin, P. E.; Gazizova, O. R.; Karpov, A. S.; Jansen, M.; Tretyakov, Y. D. *Solid State Sci.* **2007**, *9* (1), 82–87.
(74) Hoppe, R.; Baier, R.; Carl, W.; Glaum, H.; Untenecker, H. *Z. anorg. allg. Chem.* **1988**, *567*, 69.
(75) Karpov, A. S.; Nuss, J.; Jansen, M.; Kazin, P. E.; Tretyakov, Y. D. *Solid State Sci.* **2003**, *5* (9), 1277–1283.